

# Spectroscopic study of blue compact galaxies

## III. Empirical population synthesis

X. KONG<sup>1,2</sup>, S. Charlot<sup>1,3</sup>, A. Weiss<sup>1</sup>, F.Z. Cheng<sup>2</sup>

Accepted for publication in A&A: March 10, 2003

### ABSTRACT

This is the third paper of a series dedicated to the study of the star formation rates, star formation histories, metallicities and dust contents of a sample of blue compact galaxies (BCGs). We constrain the stellar contents of 73 blue compact galaxies by analyzing their continuum spectra and the equivalent widths of strong stellar absorption features using a technique of empirical population synthesis based on a library of observed star-cluster spectra. Our results indicate that blue compact galaxies are typically age-composite stellar systems; in addition to young stars, intermediate-age and old stars contribute significantly to the 5870 Å continuum emission of most galaxies in our sample. The stellar populations of blue compact galaxies also span a variety of metallicities. The ongoing episodes of star formation started typically less than a billion years ago. Some galaxies may be undergoing their first global episode of star formation, while for most galaxies in our sample, older stars are found to contribute up to half the optical emission. Our results suggest that BCGs are primarily old galaxies with discontinuous star formation histories. These results are consistent with the results from deep imaging observations of the color-magnitude diagrams of a few nearby BCGs using HST and large ground-based telescopes. The good quality of our population synthesis fits of BCG spectra allow us to estimate the contamination of the H $\alpha$ , H $\beta$ , H $\gamma$  and H $\delta$  Balmer emission lines by stellar absorption. The absorption equivalent widths measured in the synthetic spectra range from typically 1.5Å for H $\alpha$ , to 2–5Å for H $\beta$ , H $\gamma$ , and H $\delta$ . The implied accurate measurements of emission-line intensities will be used in a later study to constrain the star formation rates and gas-phase chemical element abundances of blue compact galaxies.

*Subject headings:* galaxies: compact – galaxies: evolution – galaxies: stellar component – galaxies: star clusters

---

<sup>1</sup>Max Planck Institute for Astrophysics, Karl-Schwarzschild-Str. 1, D-85741 Garching, Germany

<sup>2</sup>Center for Astrophysics, University of Science and Technology of China, 230026, Hefei, P. R. China

<sup>3</sup>Institut d'Astrophysique de Paris, CNRS, 98 bis Boulevard Arago, 75014 Paris, France

<sup>4</sup>Xu KONG : xkong@mpa-garching.mpg.de; xkong@ustc.edu.cn

## 1. Introduction

The stellar populations of galaxies carry a record of their star forming and chemical histories, from the epoch of formation to the present. The global properties of galaxies are determined by the nature and evolution of their stellar components. Their studies thus provide a powerful tool to explore the physics of galaxy formation and evolution ((Kong 2000); (Cid Fernandes et al. 2001)). For local group galaxies and some very nearby galaxies that can be resolved into individual stars with HST and 10-m class telescopes, the stellar population properties may be studied by means of direct observations. However, for objects at larger distances, individual stars (except for some giants) are unresolved, even with 10-m class telescopes. The integrated light of such galaxies is expected to contain valuable information about their physical properties.

The most common approach used to interpret the integrated spectrophotometric properties of galaxies is *stellar population synthesis*. There are two main types of population synthesis studies: evolutionary population synthesis and empirical population synthesis (EPS hereafter). Both types of studies require a complete library of input (observed or model atmosphere) spectra of stars or star clusters (e.g., (Fritze-v. Alvensleben 2000)).

In the evolutionary population synthesis approach, pioneered by Tinsley (1967), the main adjustable parameters are the stellar initial mass function (IMF), the star formation history and, in some cases, the rate of chemical enrichment. Assumptions about the time evolution of these parameters allow one to compute the age-dependent distribution of stars in the Hertzsprung-Russell diagram, from which the integrated spectral evolution of the stellar population can be obtained. In recent years, a number of groups have developed evolutionary population synthesis models, which allow one to investigate the physical properties of observed galaxies ((Bruzual 1983); Arimoto & Yoshii 1987; Buzzoni 1989; Bressan, Chiosi & Fagotto 1994; Worthey 1994; Weiss, Peletier & Matteucci 1995; Fioc & Rocca-Volmerange 1997; Mas-Hesse & Kunth 1999; Moeller, Fritze-v. Alvensleben & Fricke 1999; Leitherer et al. 1999; and Bruzual & Charlot 1993, 2003). Such models are convenient tools for studying the spectral *evolution* of galaxies, as they allow one to predict the past and future spectral appearance of galaxies observed at any given time. However, modern evolutionary population synthesis models still suffer from serious limitations (e.g., Charlot et al. 1996).

The empirical population synthesis approach, also known as ‘stellar population synthesis with a data base’, was introduced by Faber (1972). In this technique, one reproduces the integrated spectrum of a galaxy with a linear combination of spectra of individual stars or star clusters of various types taken from a comprehensive library. The empirical population synthesis approach has been employed successfully by several authors to interpret observed galaxy spectra (Faber 1972; O’Connell 1976; Pickles 1985; Bica 1988; Pelat 1998; Boisson et al. 2000; Cid Fernandes et al. 2001). An appealing property of this approach is that the results do not hinge on a priori assumptions about stellar evolution, the histories of star formation and chemical enrichment, nor—in the case of a library of individual stellar spectra—the IMF. In return, it does not allow one to predict the

past and future spectral appearance of galaxies. In 1996, a workshop devoted to the comparison of various evolutionary population synthesis and empirical population synthesis codes showed broad agreement in general and a number of discrepancies in detail (Leitherer et al. 1996).

In this paper, we use the empirical population synthesis approach to constrain the stellar content and star formation histories of a sample of 73 blue compact galaxies (BCGs). Our approach builds on earlier studies by Bica (1988) and Cid Fernandes et al. (2001), and we adopt the library of observed star-cluster spectra assembled by Bica & Alloin (1986; see also Bica 1988). Our primary goal is to illustrate the constraints that can be obtained on the ages and metallicities of the stellar populations of BCGs that cannot be resolved into individual stars, on the basis of their integrated spectra. In a forthcoming study, we will use the results of this analysis to model the spectral evolution of BCGs using evolutionary population synthesis models. Another goal of the present work is to refine previous measurements of the Balmer emission-line fluxes of the BCGs in our sample, through an accurate modeling of the underlying stellar absorption spectrum. This issue is critical to spectroscopic analyses of BCGs (e.g., (Thuan & Izotov 2000); (Olive & Skillman 2001)).

The paper is organized as follows. In Section 2, we briefly review the principle of the empirical population synthesis approach. We describe the properties of the BCG spectral sample in Section 3. In Section 4, we estimate the stellar components in BCGs by fitting the observed equivalent widths and continuum colors with the empirical population synthesis approach. In Section 5 we discuss the age-metallicity degeneracy and the possible application of our results. Section 6 summarizes our main results.

## 2. Empirical population synthesis model

In a recent paper, Cid Fernandes et al. (2001) revisit the classical problem of synthesizing the spectral properties of a galaxy by using a ‘base’ of star-cluster spectra, approaching it from a probabilistic perspective. Their work improves over previous EPS studies at both the formal and computational levels, and it represents an efficient tool for probing the stellar population mixture of galaxies. To provide a quantitative description of the stellar components in the nuclear regions of BCGs, we will apply this EPS method to our BCG sample. It is based on spectral-group templates built from star clusters of different ages and metallicities, and on Bayes probabilistic theorem and the EPS Metropolis algorithm. In this section, we first describe the star cluster base. We then briefly review Bayes probabilistic formulation and the EPS Metropolis algorithm.

### 2.1. Description of the star cluster base

Empirical population synthesis by with a data base (a base of  $n_*$  spectra of stars or star clusters) is a classical tool designed to study the stellar population of galaxies. The recent EPS algorithm of Cid Fernandes et al. (2001; see also Bica 1988) relies on a data base of star-cluster

spectra rather than on one of individual stellar spectra. The star cluster base used by Cid Fernandes et al. (2001) was introduced by Schmidt et al. (1991). It consists of 12 population groups, spanning five age bins — 10 Gyr (representing globular cluster-like populations), 1 Gyr, 100 Myr, 10 Myr and ‘HII’-type (corresponding to current star formation) — and four metallicities — 0.01, 0.1, 1 and 4 times  $Z_{\odot}$  (see Table 1 of Cid Fernandes et al. 2001). All metallicities are not available for clusters of all ages. In particular, spectra of star clusters younger than 1 Gyr are only available for the metallicities  $Z_{\odot}$  and  $4Z_{\odot}$ . Since blue compact galaxies are expected to have predominantly low abundances, the base of star-cluster spectra used by Cid Fernandes et al. (2001) is not optimal for our analysis.

The base of 35 star-cluster spectra used by Bica (1988; see also Bica & Alloin 1986) is better appropriate for our purpose, as it contains spectra of young star clusters with metallicities down to  $\log(Z/Z_{\odot}) = -0.5$  (see Table 1). Each component, corresponding to a specific age and metallicity, is characterized by a set of six metallic features (Ca II K  $\lambda 3933$ , CN  $\lambda 4200$ , G band  $\lambda 4301$ , Mg I+Mg II  $\lambda 5175$ , Ca II  $\lambda 8543$ , Ca II  $\lambda 8662$ ) and three Balmer lines (H $\delta$ , H $\gamma$ , and H $\beta$ ), as well as  $n_C = 7$  continuum fluxes at selected pivot wavelengths (3290, 3660, 4020, 4510, 6630, 7520 and 8700 Å), which are normalized at  $\lambda 5870$  Å. The library contains an HII region component corresponding to current star formation. This is represented by a pure continuum based on the spectrum of 30 Dor, which is used at all metallicities (see the recent description by Schmitt et al. 1996).

Table 1 lists the ages and metallicities of each of the 35 components of the Bica (1988) base of star-cluster spectra. The top line lists the ages of the components, while the rightmost column lists the metallicities, with  $[Z/Z_{\odot}] = \log(Z/Z_{\odot})$ .

## 2.2. The synthesis algorithm

The principle of EPS is to find the linear combination of a base of spectra ( $n_{\star}$  star clusters) that best reproduces a given set of measured observables, such as the equivalent widths  $W_j$  of  $n_W$  conspicuous absorption features and the  $n_C$  continuum fluxes  $C_k$  in an observed galaxy spectrum. Different synthesis algorithms have been developed to select the optimal combination of base spectra in the most efficient way. We use here the algorithm described by Cid Fernandes et al. (2001). Since this is relatively new, we briefly recall below its probabilistic formulation and the main features of the algorithm.

The data  $\mathcal{D}$  we wish to model is composed of a set of  $n_{obs} = n_W + n_C$  observables, as described above. The measurement errors in these observables, collectively denoted by  $\sigma$ , are known from the observations. Given these, the problem of EPS is to estimate the population vector  $\mathbf{X}$  ( $X_i$ ,  $i=1, \dots, n_{\star}$ ) and the extinction  $A_V$  that ‘best’ represents the data according to a well defined probabilistic model, where  $X_i$  denotes the fractional contribution of the  $i$ th base element to the total flux at the reference wavelength. The probability of a solution  $(\mathbf{X}, A_V)$  given the data  $\mathcal{D}$  and the errors  $\sigma$ , is given by Bayes theorem ((Smith & Grandy 1985)):

$$P(\mathbf{X}, A_V | \mathcal{D}, \sigma, \mathcal{H}) = \frac{P(\mathcal{D} | \mathbf{X}, A_V, \mathcal{H}) P(\mathbf{X}, A_V | \sigma, \mathcal{H})}{P(\mathcal{D} | \mathcal{H})}. \quad (1)$$

$\mathcal{H}$  summarizes the set of assumptions on which the inference is to be made,  $P(\mathcal{D} | \mathbf{X}, A_V, \sigma, \mathcal{H})$  is the likelihood,  $P(\mathcal{D} | \mathcal{H})$  is the normalizing constant,  $P(\mathbf{X}, A_V | \mathcal{H})$  is the joint *a priori* probability distribution of  $\mathbf{X}$  and  $A_V$ .

For a non-informative prior, the posterior probability  $P(\mathbf{X}, A_V | \mathcal{D}, \sigma, \mathcal{H})$  is simply proportional to the likelihood:

$$P(\mathbf{X}, A_V | \mathcal{D}, \sigma, \mathcal{H}) \propto P(\mathcal{D} | \mathbf{X}, A_V, \sigma, \mathcal{H}) \propto e^{-\mathcal{E}(\mathbf{X}, A_V)} \quad (2)$$

with  $\mathcal{E}$  defined as half the value of  $\chi^2$ :

$$\begin{aligned} \mathcal{E}(\mathbf{X}, A_V) &= \frac{1}{2} \chi^2(\mathbf{X}, A_V) = \frac{1}{2} \sum_{j=1}^{n_W} \left( \frac{W_j^{obs} - W_j(\mathbf{X})}{\sigma(W_j)} \right)^2 \\ &+ \frac{1}{2} \sum_{k=1}^{n_C} \left( \frac{C_k^{obs} - C_k(\mathbf{X}, A_V)}{\sigma(C_k)} \right)^2. \end{aligned} \quad (3)$$

Here  $W_j^{obs}$  and  $C_k^{obs}$  are the observed features and  $W_j(\mathbf{X})$  and  $C_k(\mathbf{X}, A_V)$  are the synthetic features.

This expression contains the full solution of the EPS problem, as embedded in it is not only the most probable model parameters but also their full probability distributions. In order to compute the individual posterior probabilities for each parameter, we use an efficient parameter-space exploration method, known as the Metropolis algorithm ((Metropolis et al. 1953)). The code preferentially visits regions of large probability, starting from an arbitrary point of the parameter space. At each iteration  $s$ , we pick one of the  $n_\star + 1$  variables at random and change it by a uniform deviate ranging from  $-\epsilon$  to  $+\epsilon$ , producing a new state  $s+1$ . Moves to states of smaller  $\chi^2$  are always accepted, whilst changes to less likely states are accepted with probability  $\exp[-(\chi_{s+1}^2 - \chi_s^2)]$ , thus avoiding trapping onto local minima. Moves towards non-physical regions ( $X_i < 0$  or  $> 1$ ,  $A_V < 0$ ) were truncated. In this way, the probability distributions for the  $X_i$  is given, and then the whole set ( $X_i, i=1, \dots, n_\star$ ) is renormalized to unit sum.

The main output of the EPS approach is the *population vector*  $\mathbf{X}$ , whose  $n_\star$  components carry the fractional contributions of each base element to the observed flux at the normalization wavelength 5870 Å. This vector corresponds to the *mean* solution found from a  $10^8$  steps likelihood-guided Metropolis walk through the parameter space. Owing to intrinsic errors in the observable parameters and some other uncertainties, more than one acceptable solution can represent the observation data. The final *mean* solution is given by the weighted ( $e^{-\chi^2/2}$ ) average of all solutions within the observational errors. This *mean* solution is more reliable than the single optimal solution, and it provides a more representative result to the population synthesis problem.

### 3. Description of the BCG sample

Our sample is drawn from the atlas of optical spectra of 97 blue compact galaxies by Kong & Cheng (2002a). The spectra were acquired with the 2.16 m telescope at the XingLong Station of the Beijing Astronomical Observatory (BAO) in China. A 300 line  $\text{mm}^{-1}$  grating was used to achieve coverage in the wavelength region from 3580 to 7600 Å with the dispersion is  $4.8 \text{ Å pixel}^{-1}$ . The slit width was adjusted in between  $2''$  and  $3''$  each night, depending on seeing conditions. A detailed description of the observations, the sample selection, the data reduction and calibration and the error analysis can be found in the first paper of this series ((Kong & Cheng 2002a)). The average signal-to-noise ratio of the spectra is  $\sim 51$  per pixel. The spectrophotometry is accurate to better than 10% over small wavelength regions and to about 15% or better on large scales.

Kong et al. (2002b) measured several quantities in the spectra of the 97 BCGs in this sample, including the fluxes and equivalent widths of emission lines, continuum fluxes, the 4000 Å break and the equivalent widths of several absorption features. The galaxies were ordered into three classes based on their emission-line properties: 13 were classified as ‘non-emission-line galaxies’ (non-ELG), 10 as ‘low-luminosity active galactic nuclei’ (AGN) and 74 as ‘star-forming galaxies’ (SFG). We are primarily interested here in the star formation rates, metallicities and star formation histories of BCGs. Therefore, we focus on the subsample of 74 star-forming galaxies (SFGs). We exclude I Zw 207 from this subsample because the absence of a blue spectrum prevents the measurements of most absorption features in this galaxy. Our final sample therefore consists of 73 star-forming, blue compact galaxies.

## 4. Empirical population synthesis results

We use the EPS approach of Cid Fernandes et al. (2001; Section 2.2 above) and the library of star-cluster spectra of Bica (1988; Section 2.1 above) to interpret the spectra of the 73 star-forming BCGs in our sample.

### 4.1. Input data

We use the following observable quantities to constrain the stellar components in the nucleus regions of BCGs: the observed absorption equivalent widths ( $W_j^{obs}$ ;  $W_j^{obs} \geq 1.0 \text{ Å}$ ) of Ca II K  $\lambda 3933$ , H $\delta$   $\lambda 4102$ , CN  $\lambda 4200$ , G band  $\lambda 4301$ , H $\gamma$   $\lambda 4340$ , and Mg I+Mg II  $\lambda 5176$  and the continuum fluxes (normalized at 5870 Å) at 3660, 4020, 4510, 6630, and 7520 Å (in practice, we use the H $\delta$  and H $\gamma$  absorption equivalent widths only for galaxies with negligible emission at these wavelengths, representing roughly half of the sample). The absorption equivalent widths and continuum fluxes were measured by Kong et al. (2002b) according to the procedure outlined in Bica (1988) and Cid Fernandes et al. (2001; see Kong et al. 2002b for detail). In some spectra, the continuum flux

at 5870 Å may be buried underneath the He I  $\lambda 5876$  Å emission line. In such cases, adjacent wavelength regions were used to estimate the continuum level. The resulting absorption equivalent widths are listed in Table 6 of Kong et al. (2002b), and the continuum fluxes in Table 4 of Kong et al. (2002b). The errors in the absorption equivalent widths and continuum fluxes must also be included as input parameters. These are set to 10% for those absorption bands with  $W_j^{obs} > 5$  Å, 20% for those absorption bands with  $1.0 < W_j^{obs} < 5$  Å, and 10% for continuum colors. These errors are consistent with the quality of the spectra (Kong & Cheng 2002a).

## 4.2. Computation

To select the linear combination of the base cluster spectra that best represents an observed galaxy spectrum, we set the EPS algorithm to sample  $N_s = 10^8$  states of the whole age versus  $[Z/Z_\odot]$  parameter space, with the ‘visitation parameter’  $\epsilon$  set to 0.05 for the  $X_i$ ’s ( $\Delta X_i = 0.05$ ) and 0.01 for  $A_V$ . As described in Section 2.2, we obtain as output a 35-dimension, *mean* population vector  $\mathbf{X}$  containing the expected values of the fractional contribution of each component to the total light at the normalization wavelength  $\lambda 5870$  and  $A_V$ . Table 2 lists, as examples, the results for two galaxies in our sample.

The results for the 73 BCGs in our sample indicate that, in all cases, a single metallicity is favored for all four youngest stellar components (corresponding to ages less than  $5 \times 10^8$  yr). The metallicity of young stars is  $[Z/Z_\odot] = -0.5$  for 55 galaxies in the sample and  $[Z/Z_\odot] = 0.0$  for the remaining 18 galaxies. For stars older than  $5 \times 10^8$  yr, the dominant metallicity anticorrelates with age, in the sense that the metallicity of the stellar component contributing most to the integrated light increases with decreasing age from  $1 \times 10^{10}$  yr to  $1 \times 10^9$  yr (see the examples in Table 2). We note that the dominant metallicity of stars older than  $5 \times 10^8$  yr is always found to be less than or equal to that of younger stars. It is not surprising that a dominant metallicity be favored for stars of any given age in a galaxy. The nuclei of BCGs correspond to small volumes, where star-forming gas is expected to be chemically homogeneous at any time. It is worth noting that our results differ from those of previous EPS analyses, such as those performed by Bica (1988) and Schmitt et al. (1996), in that we determine the evolutionary paths of galaxies in the age-metallicity plane from a full maximum-likelihood analysis. In most previous studies, the star-formation and chemical-enrichment histories of galaxies were selected from a limited number of a priori evolutionary paths.

It is of interest to exploit these results and compute simple ‘evolutionary paths’ for the galaxies in our sample. As mentioned above, for each galaxy, the EPS analysis favors a dominant metallicity for stars of any given age, such that young stars have typically a higher metallicity than older stars. At any age, however, stars of any metallicity are assigned non-zero weights by the EPS algorithm. To represent the star-formation and metal-enrichment histories of BCGs in a schematic way, we adopt for each galaxy the path favored by the EPS analysis in the age-metallicity plane. For consistency, we readjust the various proportions of stars of different ages along this path by rerunning the EPS algorithm after setting the weights of all stars outside the path to zero. Since,

Table 1: Ages (in units of yr), metallicities and numbering convention for the star clusters in the base.

HII	E7	5E7	E8	5E8	E9	5E9	E10	[Z/Z <sub>⊙</sub> ]
35	31	27	23	19	14	8	1	0.6
35	32	28	24	20	15	9	2	0.3
35	33	29	25	21	16	10	3	0.0
35	34	30	26	22	17	11	4	-0.5
					18	12	5	-1.0
						13	6	-1.5
							7	-2.0

Table 2: Empirical population synthesis results of percentage contributions from stars of all ages and metallicities to  $F_{\lambda 5870}$ , for two sample galaxies. The ‘evolutionary paths’ favored by the analysis are highlighted (see text).

a) Mrk 385									b) I Zw 97								
Age (yr)									Age (yr)								
HII	E7	5E7	E8	5E8	E9	5E9	E10	[Z/Z <sub>⊙</sub> ]	HII	E7	5E7	E8	5E8	E9	5E9	E10	[Z/Z <sub>⊙</sub> ]
	2.0	1.8	2.1	.3	.2	.2	.5	0.6		.3	1.6	2.6	1.7	.3	.2	.1	0.6
	2.1	2.3	2.9	.5	.3	.3	.6	0.3		.4	1.9	3.3	3.0	.6	.3	.1	0.3
	1.5	3.3	3.9	.8	.5	.5	.8	0.0	<b>8.0</b>	<b>.8</b>	<b>5.9</b>	<b>9.8</b>	<b>5.9</b>	1.7	.6	.2	0.0
<b>8.8</b>	<b>4.0</b>	<b>6.0</b>	<b>6.9</b>	<b>11.7</b>	1.7	1.5	1.8	-0.5		.5	1.9	3.3	1.8	2.8	1.2	.7	-0.5
					<b>4.5</b>	3.4	3.4	-1.0						<b>4.7</b>	1.9	1.5	-1.0
						<b>5.5</b>	5.4	-1.5							<b>6.9</b>	7.0	-1.5
							<b>8.1</b>	-2.0								<b>16.7</b>	-2.0



for a given galaxy, the age-metallicity space to be explored then reduces to a single dimension, we refine the analysis by lowering the ‘visitation parameter’  $\epsilon$  to 0.005 ( $\Delta X_i = \mathbf{0.005}$ ) while still sampling  $N_s = 10^8$  states (we keep  $\epsilon = 0.01$  for  $A_V$ ).

### 4.3. Stellar populations

The results of our analysis are summarized in Tables 3 and 4 for the galaxies with asymptotic (young-star) metallicities  $[Z/Z_\odot] = -0.5$  and  $0.0$ , respectively. For each galaxy, we report the percentage contributions from each age-metallicity component to the integrated flux at  $\lambda = 5870$  Å. The first and second lines of each table indicate the metallicities and the ages of the different stellar components. For reference, the third line indicates the indices of the stellar components in the cluster data base of Table 1. For each galaxy, we also list the inferred  $V$ -band attenuation  $A_V$  and the absorption equivalent widths of  $H\gamma$ ,  $H\delta$ ,  $H\beta$  and  $H\alpha$ , as measured from the synthetic stellar population spectra. Figure 1 shows the equivalent widths ( $W_j^{syn}$ ) of all the stellar absorption features used to constrain the fits in the model spectra against those in the observed spectra ( $W_j^{obs}$ , for  $W_j^{obs} \geq 1.0$  Å), for all 73 BCGs in our sample. Clearly, the feature strengths in the model spectra are in very good agreement with those in the observed spectra.

A first noticeable result in Tables 3 and 4 is that all BCGs show an underlying component of stars older than  $1 \times 10^9$ yr. The fractional contribution of this component to the total light at  $\lambda 5870$  Å exceeds 15% for most galaxies, except for some low-luminosity BCGs, such as I Zw 18, II Zw 40, which have very strong emission line spectra, and have a marginally detected old component. We note that the spectra used here sample the inner regions of the galaxies. The contribution from old and intermediate-age stars to the integrated light could be even larger in the extended (off-nuclear) regions of galaxies. The presence of significant populations of old and intermediate-age stars indicates that blue compact galaxies have experienced substantial episodes of star formation in the past. This supports the results from deep imaging observations of the color-magnitude diagrams of a few nearby BCGs that these are old galaxies (see section 5.2 below). As expected, stars younger than  $5 \times 10^8$ yr tend to dominate the emission at  $5870$  Å, consistent with the observational character of BCGs, i.e. blue colors and strong emission lines.

Another interesting result of Tables 3 and 4 is that blue compact galaxies present a variety of star formation histories. In II Zw 67 and I Zw 56, for example, stars with age 10 Gyr contribute as much as 20 per cent of the flux at  $\lambda 5870$  Å. In contrast, in III Zw 43 and Mrk 57, old stars do not contribute significantly to the flux at  $\lambda 5870$  Å, that is produced in half by intermediate-age stars. The galaxies I Zw 18 and II Zw 40 differ from these cases in that their emission at  $\lambda 5870$  Å is accounted almost entirely by young stars. The star formation history of BCGs, therefore, appears to vary significantly on a case by case basis.

For simplicity, in what follows we arrange stars into four age bins: **OLD** stars with age  $1 \times 10^{10}$ yr (proportion  $\mathbf{X}_{OLD}$ ); **INT**ermediate-age stars with ages between  $1 \times 10^9$ yr and  $5 \times 10^9$ yr

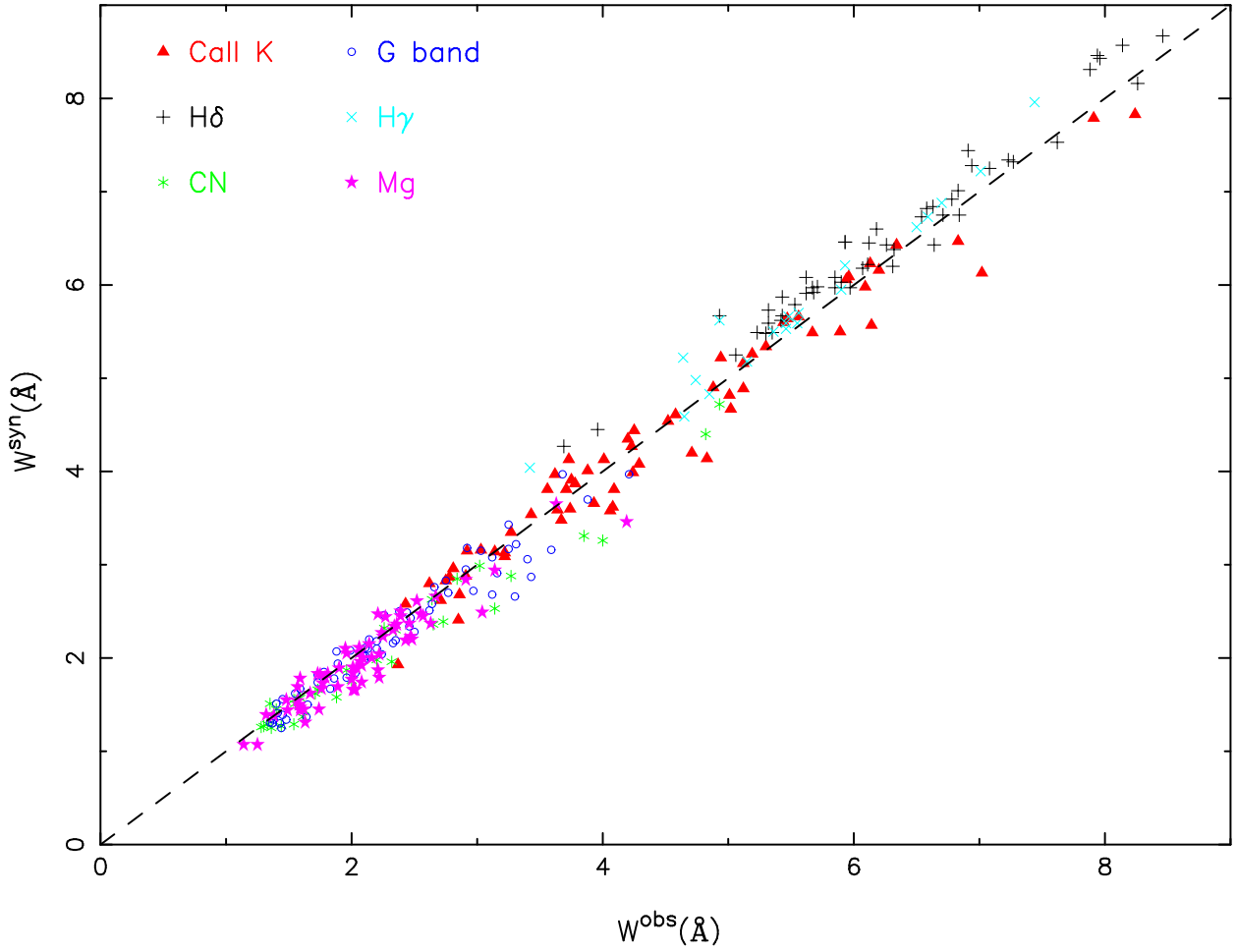


Fig. 1.— Synthetic equivalent width  $W^{syn}$  against observed equivalent width  $W^{obs}$  for all  $W_j^{obs} \geq 1.0 \text{ \AA}$  absorption features used to constrain the star-formation and chemical-enrichment histories of 73 BCGs (see Tables 3 and 4). The dash line is the identity line. Different symbols denote different absorption features, as indicated.

Table 3: Empirical population synthesis results of the galaxies with asymptotic (young-star) metallicities  $[Z/Z_{\odot}]=-0.5$ : percentage contribution to  $F_{\lambda 5870}$ .

[Z/Z <sub>⊙</sub> ]	[Z/Z <sub>⊙</sub> ]=-0.5								EW <sub>abs</sub> (Å)					
	Age(yr)	HII	E7	5E7	E8	5E8	-1.0	-1.5	-2.0	A <sub>V</sub>	Hδ	Hγ	Hβ	Hα
Name	35	34	30	26	22	18	13	7						
iiizw12	18.2	10.0	16.2	10.5	10.9	18.9	9.6	5.6	.07	4.62	3.50	4.09	1.51	
haro15	23.3	5.7	19.8	20.8	13.5	9.8	4.0	3.2	.04	4.59	3.27	3.75	1.51	
iiizw33	21.3	5.4	10.7	8.2	18.5	16.5	11.3	8.1	.08	3.78	2.44	3.56	1.38	
iiizw43	1.0	1.6	4.6	6.1	21.4	43.0	16.4	6.0	.86	4.24	3.45	4.33	1.25	
iizw23	14.1	6.0	14.4	10.2	8.4	18.0	19.6	9.3	.27	4.76	3.17	4.26	1.89	
iizw28	28.1	6.3	10.6	7.8	19.8	14.4	7.6	5.5	.06	3.41	2.19	3.09	1.03	
iizw33	27.3	3.5	5.1	3.0	6.4	24.0	22.6	8.1	.09	3.01	1.88	2.94	1.59	
iizw40	52.4	1.8	11.9	13.1	13.5	4.8	1.4	1.2	.01	2.57	2.11	2.23	.66	
mrk5	12.1	2.3	7.2	9.2	48.6	14.6	3.1	2.9	.02	3.57	3.20	4.43	.28	
viizw153	9.2	5.1	14.8	11.3	24.1	23.6	7.3	4.6	.05	4.70	3.81	4.36	1.53	
viizw156	2.6	2.8	16.3	15.8	17.5	16.4	17.8	10.9	.17	5.53	4.02	4.55	1.71	
haro1	21.7	6.8	14.8	18.6	15.2	9.8	6.1	6.9	.09	4.37	3.12	4.76	1.82	
mrk385	9.0	6.7	16.4	14.3	22.6	13.3	9.2	8.6	.10	5.03	2.48	4.60	1.39	
mrk390	25.0	7.7	14.7	10.3	8.6	18.1	10.4	5.4	.11	4.08	2.84	3.81	1.93	
mrk105	8.5	9.5	8.5	8.8	12.9	25.0	16.2	10.6	.41	4.69	3.34	4.25	1.50	
izw18	47.8	1.1	6.9	10.5	26.9	4.5	1.2	1.1	.01	2.25	1.87	2.31	.29	
mrk402	23.5	7.1	12.9	7.7	14.7	24.4	6.3	3.4	.04	3.80	3.10	3.49	1.63	
haro22	27.0	3.9	20.1	15.5	9.0	11.0	7.7	5.9	.06	4.29	3.35	3.47	1.55	
haro23	28.4	3.2	12.4	9.5	19.6	19.0	4.7	3.3	.03	3.39	2.64	3.35	1.01	
haro2	32.6	5.5	15.0	13.5	14.2	13.0	3.6	2.6	.03	3.63	2.77	3.45	1.64	
mrk148	16.6	4.3	12.5	9.2	8.7	10.1	21.0	17.6	.84	4.39	2.57	3.98	1.69	
haro25	26.5	7.4	14.5	15.5	10.4	8.4	7.9	9.5	.10	4.11	3.27	3.84	1.30	
mrk1267	20.6	4.3	15.8	16.3	26.0	9.9	3.8	3.3	.03	4.22	3.08	3.96	.89	
haro4	45.6	3.6	18.9	14.5	8.0	5.6	2.1	1.7	.02	3.34	2.66	2.93	1.00	
mrk169	16.3	9.2	10.2	6.6	7.7	14.8	22.9	12.2	.61	4.43	3.07	4.59	1.88	
haro27	13.9	4.1	6.8	4.5	14.7	35.8	13.2	7.0	.07	3.66	2.67	3.23	1.72	
mrk201	24.5	4.2	12.8	15.1	11.6	11.6	9.4	10.7	.12	3.96	3.11	4.02	1.61	
haro28	4.2	3.7	7.6	5.4	12.5	31.6	25.1	9.8	.09	4.69	2.03	3.94	1.44	
haro8	11.7	2.0	8.3	8.3	30.6	36.2	1.8	1.2	.01	3.63	3.14	3.91	.80	
haro29	37.4	2.0	12.4	11.9	25.3	7.7	1.8	1.4	.01	3.04	2.49	3.12	.78	
mrk215	19.9	8.7	11.2	8.5	15.0	14.8	12.3	9.7	.10	4.09	3.11	4.39	1.67	
haro32	36.9	5.2	12.9	9.2	8.2	16.2	6.9	4.4	.05	3.23	2.23	2.66	1.28	
haro33	21.3	2.5	17.8	16.3	23.9	12.1	3.4	2.7	.03	4.23	3.20	3.18	1.24	
haro36	7.8	2.8	8.4	6.7	43.3	23.6	4.2	3.2	.02	3.83	1.54	3.59	.52	
haro35	19.7	4.4	17.2	17.8	14.6	14.5	6.3	5.4	.05	4.50	3.66	4.54	1.27	
haro37	25.7	6.9	16.5	12.9	14.8	12.1	6.4	4.7	.05	4.12	3.23	3.39	1.30	
mrk57	.6	1.0	3.1	3.7	29.0	37.5	20.0	5.2	.17	4.02	2.60	3.77	1.09	
mrk235	15.2	4.4	7.4	5.8	10.4	20.2	23.0	13.6	.14	3.98	2.82	3.40	1.53	
haro38	12.4	2.8	14.2	11.4	33.5	18.0	4.3	3.4	.03	4.25	2.88	3.31	1.19	
mrk275	20.0	3.9	12.2	7.0	19.7	23.4	8.7	5.1	.05	3.77	2.60	3.42	1.25	
haro42	23.3	3.1	9.8	7.9	9.7	22.6	14.3	9.3	.07	3.58	2.73	3.22	1.32	
haro43	10.0	3.8	17.0	12.1	29.3	18.8	5.2	3.8	.03	4.69	3.30	4.23	1.32	
haro44	25.9	4.4	20.8	15.7	18.5	9.6	3.0	2.1	.02	4.28	3.65	3.54	1.11	
iizw70	38.2	4.1	13.1	10.5	19.4	9.9	2.8	2.1	.02	3.11	2.67	3.02	.84	
izw117	22.3	7.0	13.1	11.2	8.8	11.4	14.0	12.1	.56	4.18	3.47	3.76	1.43	
izw123	26.6	3.9	12.2	12.7	27.2	9.7	4.0	3.7	.03	3.58	1.58	3.82	1.10	
mrk297	31.6	3.4	12.6	14.9	16.0	9.1	5.7	6.8	.06	3.52	2.51	3.63	1.51	
izw159	22.0	6.8	11.7	10.3	23.1	17.4	5.2	3.7	.04	3.81	2.98	3.60	1.27	
izw166	25.1	7.6	15.6	11.7	8.8	8.6	11.7	10.8	.27	4.21	2.23	4.03	1.85	
mrk893	15.7	6.2	10.4	7.6	12.9	20.3	16.5	10.5	.16	4.19	2.83	3.51	1.98	
izw191	5.0	8.8	7.5	7.1	14.6	33.6	15.3	8.0	.19	4.71	3.88	3.92	1.49	
ivzw93	22.5	5.0	12.6	7.7	12.9	25.3	9.4	4.7	.05	3.79	2.56	3.51	1.82	
mrk314	22.6	4.1	14.9	10.1	9.7	11.6	14.7	12.2	.16	4.13	2.22	2.78	1.57	
ivzw149	16.0	4.9	16.6	14.8	23.7	16.0	4.5	3.5	.03	4.49	3.40	4.17	1.44	
zw2335	16.5	4.9	11.1	9.2	11.3	13.4	19.3	14.4	.34	4.27	3.26	3.92	1.58	

(proportion  $\mathbf{X}_{\text{INT}}$ ); **Young Stars** with ages between  $10^7\text{yr}$  and  $5 \times 10^8\text{yr}$  (proportion  $\mathbf{X}_{\text{YS}}$ ); and newly-born stars in H II regions (proportion  $\mathbf{X}_{\text{HII}}$ ). Hence  $\mathbf{X}_{\text{OLD}} + \mathbf{X}_{\text{INT}} + \mathbf{X}_{\text{YS}} + \mathbf{X}_{\text{HII}} = 1$ . Figure 2 illustrates graphically the variety of star formation histories reported in Tables 3 and 4 for the 73 galaxies in our sample. In each panel, the horizontal axis represents  $\mathbf{X}_{\text{HII}}$ ,  $\mathbf{X}_{\text{YS}}$ ,  $\mathbf{X}_{\text{INT}}$ , and  $\mathbf{X}_{\text{OLD}}$  (from left to right), while the vertical axis shows the percentage contributions at  $5870\text{\AA}$  of stars in these four age bins. Stars younger than  $5 \times 10^8\text{yr}$  dominate the emission in most BCGs, but the galaxies also contain substantial fractions of older stars.

#### 4.4. Spectral fits

Figure 3 illustrates the results of the spectral fits obtained for four galaxies in our sample. Also shown are the contributions to the integrated spectrum by stars in the four age groups defined in section 4.3 above (the relative contributions by the different stellar components to the total flux at  $\lambda 5870\text{ \AA}$  are those listed in Tables 3 and 4 for these galaxies). Figure 3 shows that the synthetic spectra (**SYN**) inferred from our population synthesis analysis provide good fits to the observed spectra of BCGs (**OBS**). The absorption wings of H $\beta$ , H $\gamma$  and H $\delta$  in the observed spectra are also well reproduced by the models (the synthetic spectra do not include nebular emission lines). We find that, for some strong star-forming galaxies, the synthetic spectra do not provide very good fits to the observed continuum spectra at wavelengths between 4300 and 4800  $\text{\AA}$ . This may arise from the presence of Wolf-Rayet (WR) features, such as N III features at  $\lambda 4511 - 4535$ , [N II] $\lambda 4565$ , [N V] $\lambda 4605$ ,  $4620$ , and He II $\lambda 4686$ , in the observed spectra. We plan to investigate this small discrepancy using evolutionary population synthesis models in a future paper.

#### 4.5. Evolutionary diagram

The range of star formation histories inferred for the BCGs in our sample may be interpreted in terms of an evolutionary sequence. Following Cid Fernandes et al. (2001b), we represent graphically the histories of star formation of the galaxies in Figure 4, in a plane with abscissa  $\mathbf{X}_{\text{H+Y}} = \mathbf{X}_{\text{HII}} + \mathbf{X}_{\text{YS}}$  and ordinate  $\mathbf{X}_{\text{INT}}$ . Also shown as dashed lines in the figure are lines of constant  $\mathbf{X}_{\text{OLD}}$  ( $\mathbf{X}_{\text{H+Y}} + \mathbf{X}_{\text{INT}} + \mathbf{X}_{\text{OLD}} = 1$ ).

The main result from Figure 4 is that the 73 BCGs in our sample define a sequence in  $\mathbf{X}_{\text{H+Y}}$  and  $\mathbf{X}_{\text{INT}}$  over a relatively small range of  $\mathbf{X}_{\text{OLD}}$ . The range in  $\mathbf{X}_{\text{OLD}}$  is slightly smaller for galaxies with asymptotic (young-star) metallicity  $[Z/Z_{\odot}] = -0.5$  (stars) than for those with asymptotic metallicity  $[Z/Z_{\odot}] = 0.0$  (squares). Some galaxies with ‘extreme’ stellar populations are labelled in Fig. 4. In I Zw 56 and II Zw 67, for example, old stars contribute up to  $\sim 20\%$  of the integrated flux at  $\lambda 5870$  (see section 4.3 above). The galaxy III Zw 43 is that where intermediate-age stars contribute the most to the optical continuum emission. In contrast, some galaxies, such as I Zw 18, II Zw 40, appear to be almost ‘pure starbursts’. The small percentage of old and intermediate-age stars found

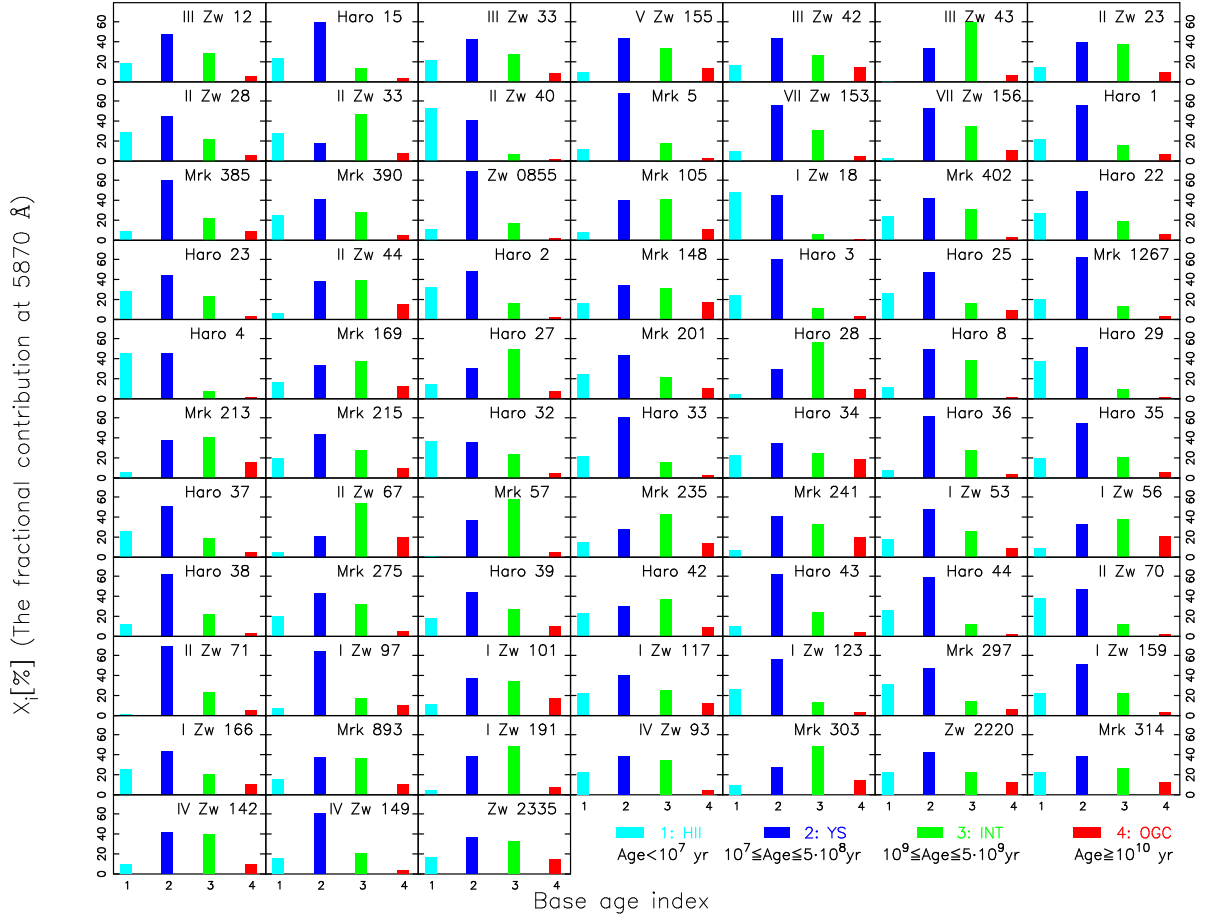


Fig. 2.— Star formation histories of 73 BCGs. In each panel, the numbers on the horizontal axis represent the stellar age groups, as indicated in the bottom right of the figure. The vertical axis shows the percentage contributions of stars in the various age groups to the integrated flux at  $5870\text{\AA}$ .

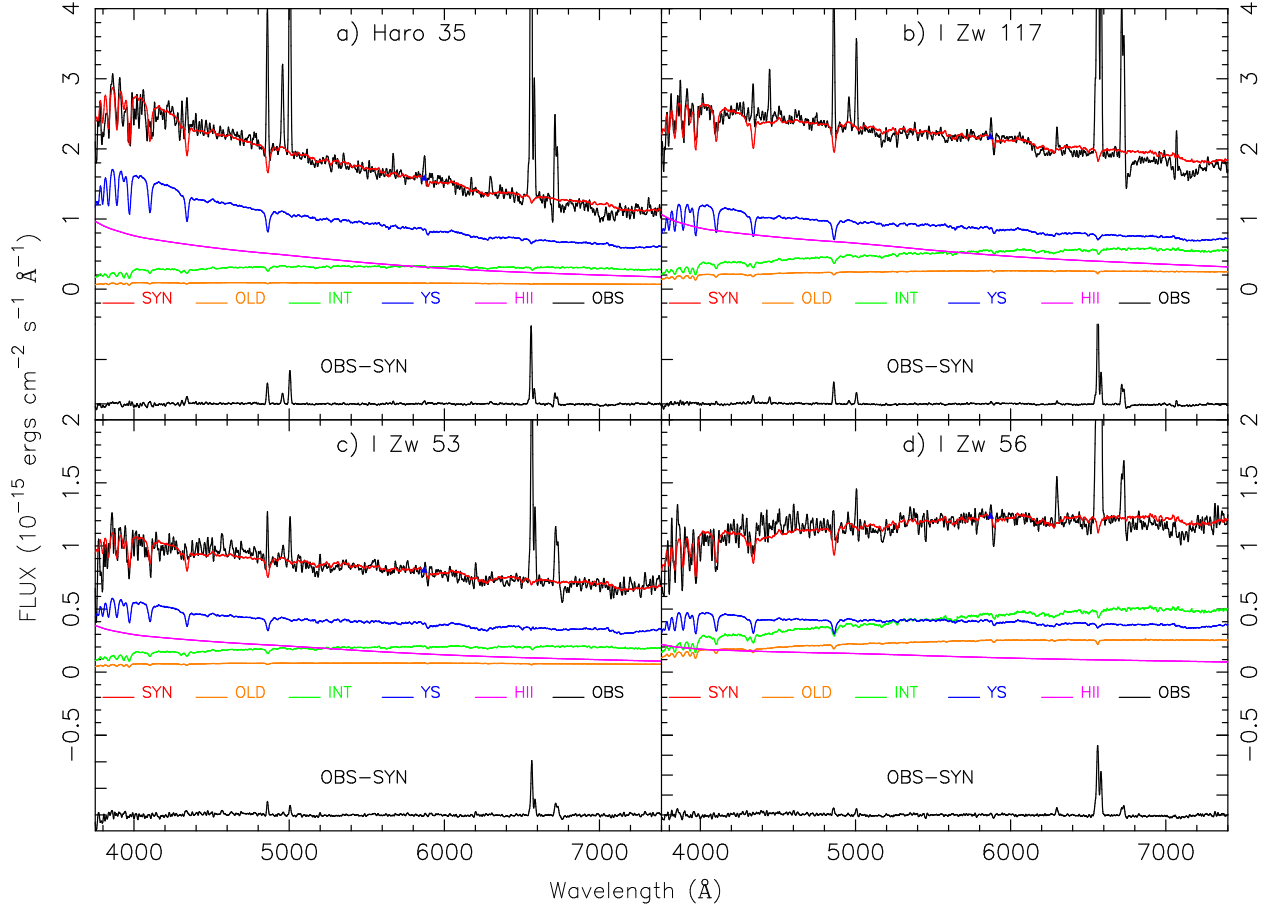


Fig. 3.— Comparison of synthetic spectra (red-solid lines) to the observed spectra of four BCGs (corrected for Galactic reddening; black-solid lines): Haro 35, I Zw 117, I Zw 53, and I Zw 56. The contributions to the synthetic spectra by old stars (OLD,  $10^{10}$ yr), intermediate-age stars (INT,  $10^9$ ,  $5 \times 10^9$ yr), young stars (YS,  $10^7 - 5 \times 10^9$ yr), and newly-born stars (H II) are also shown. The emission line spectrum appears in the OBS-SYN difference, at the bottom of each panel.

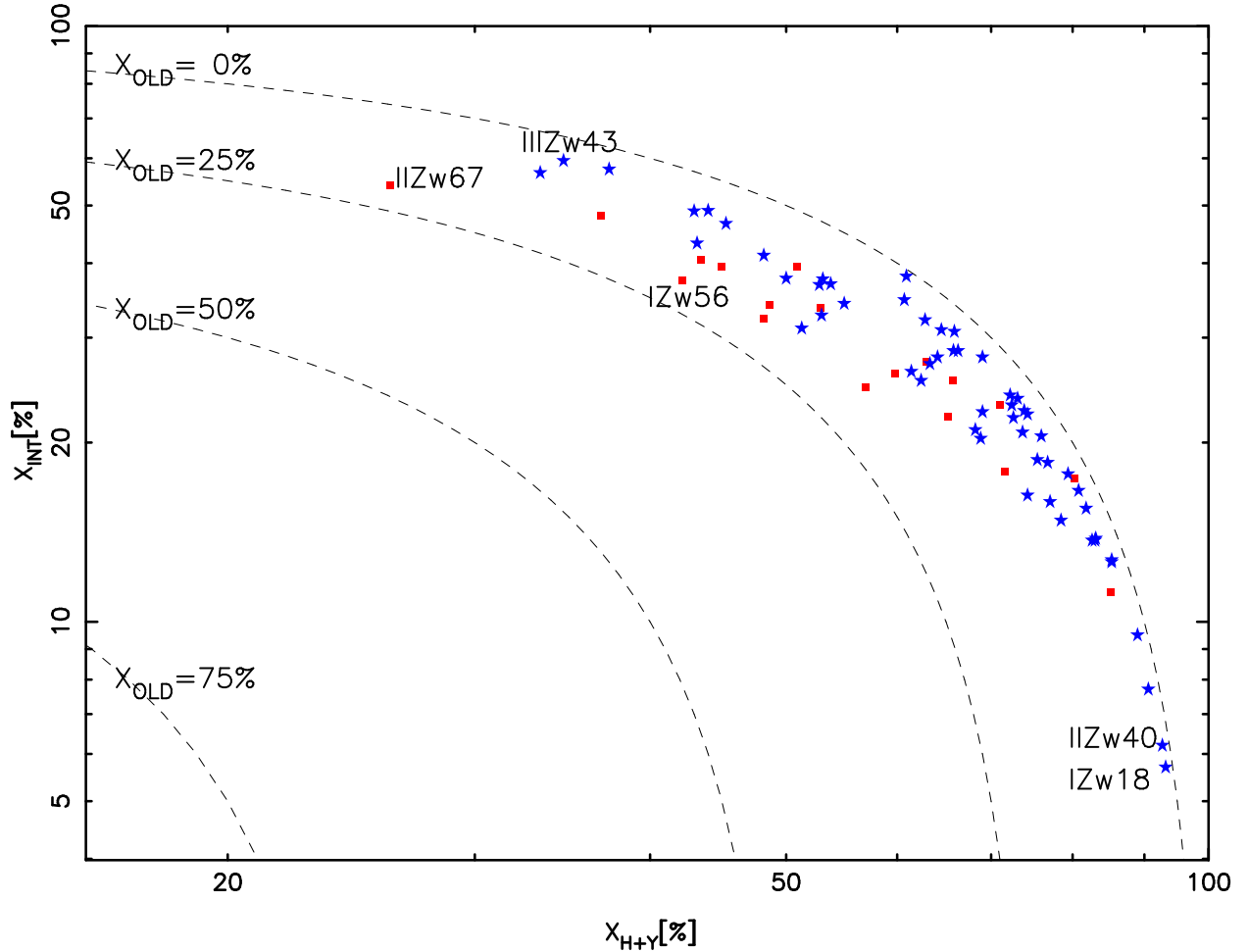


Fig. 4.— Results of the empirical population synthesis analysis for the galaxies with asymptotic (young-star) metallicities  $[Z/Z_{\odot}] = -0.5$  (stars) and  $0.0$  (squares), condensed on an evolutionary diagram. The horizontal axis  $\mathbf{X}_{H+Y} = \mathbf{X}_{HII} + \mathbf{X}_{YS}$  is the fraction of light at  $\lambda 5870 \text{ \AA}$  due to star clusters between the  $10^7$  and  $5 \times 10^8 \text{ yr}$  age bins and H II regions, while the fraction  $\mathbf{X}_{INT}$  due to stars in the  $10^9$  and  $5 \times 10^9 \text{ yr}$  age bins is plotted along the vertical axis. Dotted lines indicate lines of constant  $\mathbf{X}_{OLD}$  ( $10^{10} \text{ yr}$ ), as labeled.

here for these galaxies is consistent with the results from other recent studies, e.g., Smoker et al. (1999), Aloisi et al. (1999) (see section 5.2 below).

Since the location of an individual galaxy in Figure 4 reflects the evolutionary state of its stellar population, we can interpret the *distribution* of galaxies in this diagram as an *evolutionary* sequence. In particular, starbursting galaxies whose spectra are entirely dominated by young massive stars (bottom right part of the diagram) will presumably evolve toward larger  $\mathbf{X}_{\text{INT}}/\mathbf{X}_{\text{H+Y}}$  values (top left part of the diagram) over a timescale of a few  $10^9$ yr, once their bursts have ceased. This interpretation is supported by several observational facts. First, metal absorption-line features become stronger and galaxy colors become progressively redder as one moves from large  $\mathbf{X}_{\text{H+Y}}$  to large  $\mathbf{X}_{\text{INT}}$  along the sequence. Second, galaxies with large  $\mathbf{X}_{\text{OLD}}$  (such as I Zw 56, II Zw 67) have spectra typical of a “post-starburst” galaxies, with pronounced Balmer absorption lines characteristic of A-type stars and with no strong emission lines. Finally, most BCGs in which WR features have been detected are located in the large- $\mathbf{X}_{\text{H+Y}}$  region of the diagram, consistent with the young burst ages implied by the presence of WR stars ((Schaerer et al. 1999)).

#### 4.6. Stellar Balmer absorption

Accurate measurements of the H-Balmer emission lines are crucial to constrain the attenuation by dust, the star formation rate, the gas-phase abundances of chemical elements and the excitation parameter in galaxies (e.g., (Rosa-González et al. 2002)). To measure with accuracy the Balmer emission-line fluxes of BCGs, we must account for the contamination by underlying stellar absorption.

Different approaches have been used to correct Balmer emission-line fluxes for underlying stellar absorption in BCGs. The simplest approach consists in adopting a constant equivalent width (1.5–2 Å) for all the Balmer absorption lines (e.g., (Skillman & Kennicutt 1993); (Popescu & Hopp 2000)). Another standard correction consists in determining the absorption equivalent width through an iterative procedure, by assuming that the equivalent width is the same for all Balmer lines and by requiring that the color excesses derived from  $\text{H}\alpha/\text{H}\beta$ ,  $\text{H}\beta/\text{H}\gamma$ , and  $\text{H}\beta/\text{H}\delta$  be consistent (e.g., (Olive & Skillman 2001); (Cairós et al. 2002)). In reality, however, the absorption equivalent width may not be the same for all H-Balmer lines.

The advantage of the empirical population synthesis method used above to fit the observed spectra of BCGs is that it provides simultaneous fits to the continuum and stellar absorption features of the galaxies. We have measured the absorption equivalent widths of  $\text{H}\alpha$ ,  $\text{H}\beta$ ,  $\text{H}\gamma$ , and  $\text{H}\delta$  in the synthetic spectra fitted to all 73 galaxies in our sample (last four columns of Table 3 and 4). Figure 5 shows the distributions of the equivalent widths of the four lines. The equivalent widths of  $\text{H}\gamma$ ,  $\text{H}\delta$ , and  $\text{H}\beta$  range typically between 2 Å and 5 Å (the distributions have different shapes for different lines), while that of  $\text{H}\alpha$  is typically less than 2 Å. Hence, Figure 5 indicates that adopting a constant absorption equivalent width for all H-Balmer lines is only a crude approximation. Our



results are consistent with those of Mas-Hesse & Kunth (1999) and Olofsson (1995).

We can correct with accuracy, therefore, the fluxes of Balmer emission lines for underlying stellar absorption in the spectra of BCGs. In a forthcoming study, we will exploit the nebular emission-line spectra (OBS-SYN in Figure 3) of BCGs to constrain the rates of star formation and gas-phase chemical element abundances in these galaxies.

## 5. Discussion

### 5.1. Age-metallicity degeneracy

It is worth noting that the reason why we are able to constrain simultaneously the ages and metallicities of the different stellar components in BCGs is that our approach is based on fitting stellar absorption lines, in addition to continuum fluxes. Age and metallicity have similar effects on the continuum spectra of galaxies. However, some stellar absorption features such as  $H\beta$ ,  $H\delta$ ,  $H\gamma$  and the G-band have been shown to depend mostly on age, while others, such as  $Mg\text{I}+Mg\text{H}$  and  $Fe\lambda 5709$ , have been shown to depend mostly on metallicity (e.g., (Worthey & Ottaviani 1997); (Vazdekis & Arimoto 1999); (Kong & Cheng 2001)).

In this paper, we use the  $Ca\text{II K } \lambda 3933$ ,  $H\delta \lambda 4102$ ,  $CN \lambda 4200$ , G band  $\lambda 4301$ ,  $H\gamma \lambda 4340$  and  $Mg\text{I}+Mg\text{H } \lambda 5176$  absorption features to determine the stellar population of BCGs. These include both age-sensitive and metal-sensitive features. Some of these absorption features may not be available in some spectra, which may lack, for example,  $H\delta$  and  $H\gamma$ . Also, some absorption features may be very shallow, and hence difficult to measure with high accuracy. For most galaxies, however, we find that the results of the empirical population synthesis analysis provide coarse but useful constraints on the histories of star formation and metal enrichment.

### 5.2. Population synthesis versus CMD analysis

The most straightforward way to observe the star formation history of galaxies is through deep single-star photometry. This allows one to directly identify stars in various evolutionary phases through their positions in a color-magnitude diagram (CMD) containing the fossil record of the star formation history. During the past few years, intense activity has focused on the reconstruction of the star formation histories of nearby galaxies using this approach. Several of these studies were performed on BCGs and led to new constraints on the ages of the oldest stars present in these galaxies ((Aloisi et al. 1999); (Crone et al. 2002); (Papaderos et al. 2002); (Oestlin et al. 1998)). The general conclusions from these studies are that BCGs contain evolved stellar populations, and that their star formation histories have been discontinuous. The basic shortcoming of this approach is that it cannot be used in galaxies at large distances. In addition, the CMD-analysis method is also subject to several uncertainties such as distance determination, extinction, and contamination

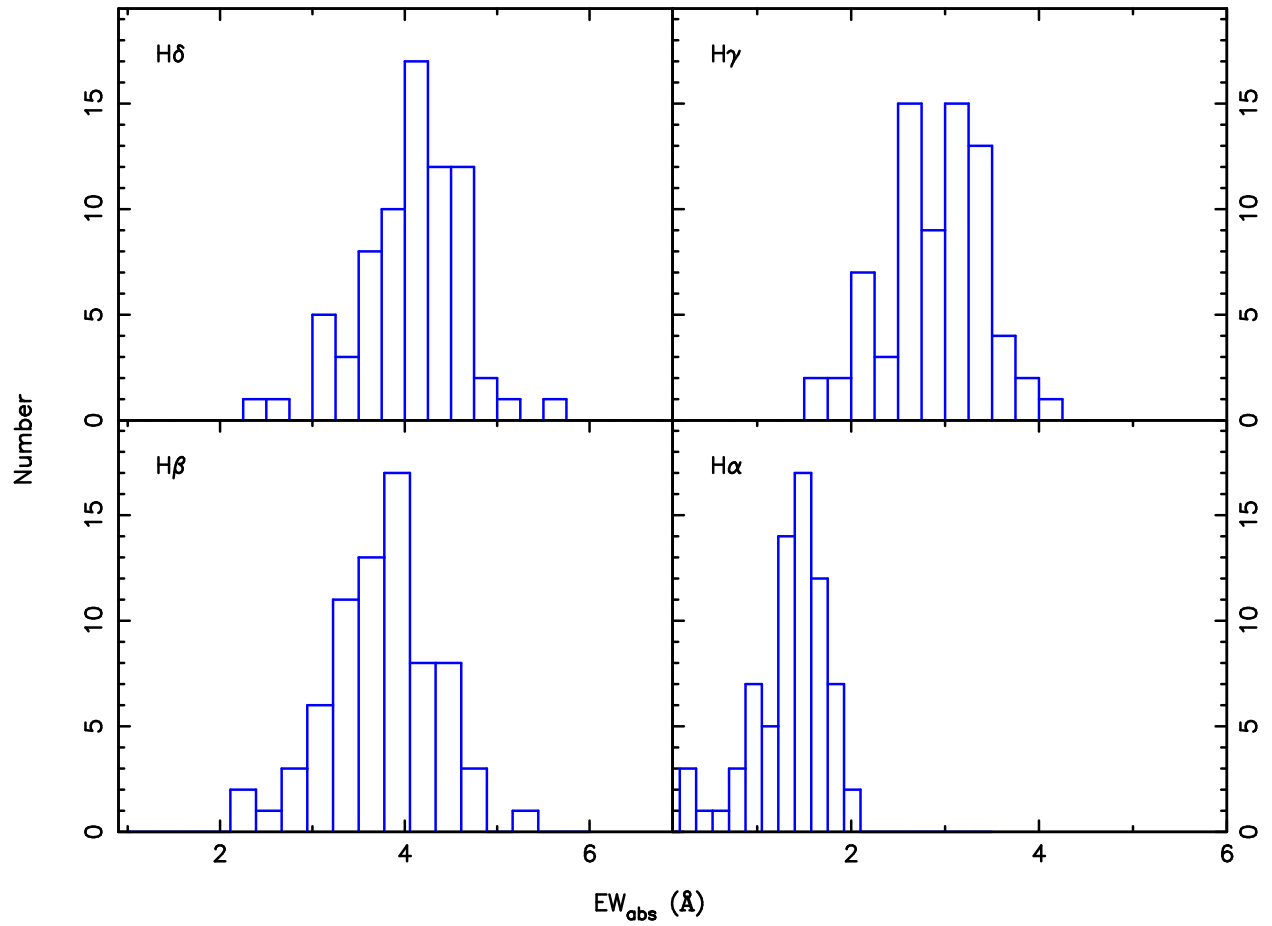


Fig. 5.— Distribution of the equivalent widths (in units of Å) for the underlying Balmer absorption features, which were measured from the synthetic stellar population spectrum.

of stellar colors by gaseous emission.

Our results of the EPS analysis of 73 BCGs are consistent with those of the CMD analysis of a few nearby galaxies, supporting the finding that BCGs are old galaxies with intermittent star formation. The evolutionary diagram constructed in Figure 4 above shows that the EPS method is not only able to recognize composite systems from a handful of observable absorption-line features and continuum fluxes, but also to provide a rough description of the evolutionary state of the stellar components. Therefore, the EPS method provides a convenient tool for the study of stellar components and star formation histories of galaxies. It can be easily applied to the spectra gathered by large spectroscopic galaxy surveys.

## 6. Summary

We have presented the results of an empirical population synthesis study of a sample of 73 blue compact galaxies. Our main goal was to study the stellar components of BCGs. We have constrained the star formation histories of BCGs by comparing observed stellar absorption features and continuum fluxes with a library of star cluster spectra. Our conclusions can be summarized as follows:

BCGs present a variety of star formation histories, as inferred from the wide spread in stellar absorption equivalent widths and continuum colors from galaxy to galaxy. BCGs are typically age-composite stellar systems, in which different stellar components are clearly distinguished: the current starburst, an underlying older population, and some intermediate-age population.

A quantitative analysis indicates that the nuclei of some BCGs are dominated by young components and the star-forming process is still ongoing. In most of BCGs, stars older than 1 Gyr contribute significantly to the integrated optical emission. The contribution by these stars can exceed 40% in some cases. Overall, the stellar populations of BCGs suggest that they are old galaxies undergoing intermittent star formation episodes; a typical BCGs is not presently forming its first generation of stars. We also find that the attenuation by dust is typically very small in the BCGs in our sample.

Our results are consistent with the results from deep imaging observations using HST and large ground-based telescopes. The virtue of the EPS approach is that it is applied to integrated galaxy spectra. This method should be useful, therefore, for interpreting the spectra gathered by large spectroscopic galaxy surveys.

The EPS approach also provides accurate spectral fits of observed galaxy spectra. From these spectral fits, it is possible to measure with accuracy, in particular, the absorption strengths of stellar Balmer lines and to correct the observed Balmer emission-line fluxes for underlying stellar absorption. The pure emission-line spectra of the BCGs in our sample, resulting from the subtraction of the synthetic spectral fits from the observed spectra, will be presented in a forthcoming paper.

We thank an anonymous referee for helpful comments and constructive suggestions, which helped us improve the paper. We are very grateful to Dr. R. Cid Fernandes for giving us the EPS computer program, and kindly assisting us in its use. This work is based on observations made with the 2.16m telescope of the Beijing Astronomical Observatory(BAO) and supported by the Chinese National Natural Science Foundation (CNNSF 10073009). S.C. thanks the Alexander von Humboldt Foundation, the Federal Ministry of Education and Research, and the Programme for Investment in the Future (ZIP) of the German Government for support. X.K. has been financed by the Special Funds for Major State Basic Research Projects of China and the Alexander von Humboldt Foundation of Germany.

### REFERENCES

- Alloin, D., Gallart, C., Fleurence, E., et al. 2002, *Ap&SS*, 281, 109
- Aloisi, A., Tosi, M., & Greggio, L. 1999, *AJ*, 118, 302
- Arimoto, N. & Yoshii, Y. 1987, *A&A*, 173, 23
- Bergvall, N. & Östlin, G. 2002, *A&A*, 390, 891
- Bica, E. 1988, *A&A*, 195, 76
- Bica, E. & Alloin, D. 1986, *A&A*, 162, 21
- Boisson, C., Joly, M., Moultaq, J., et al. 2000, *A&A*, 357, 850
- Bressan, A., Chiosi, C., & Fagotto, F. 1994, *ApJS*, 94, 63
- Bruzual A., G. 1983, *ApJ*, 273, 105
- Bruzual, A. G. & Charlot, S. 1993, *ApJ*, 405, 538
- Bruzual, A. G. & Charlot, S. 2003, *MNRAS*, submitted.
- Buzzoni, A. 1989, *ApJS*, 71, 817
- Cairós, L. M., Caon, N., García-Lorenzo, B., et al. 2002, *ApJ*, 577, 164
- Charlot, S., Worthey, G., & Bressan, A. 1996, *ApJ*, 457, 625
- Cid Fernandes, R., Sodré, L., Schmitt, H. R., et al. 2001, *MNRAS*, 325, 60
- Cid Fernandes, R., Heckman, T., Schmitt, H., et al. 2001b, *ApJ*, 558, 81
- Crone, M. M., Schulte-Ladbeck, R. E., Greggio, L., & Hopp, U. 2002, *ApJ*, 567, 258
- Faber, S. M. 1972, *A&A*, 20, 361

- Fioc, M. & Rocca-Volmerange, B. 1997, *A&A*, 326, 950
- Fritze-v. Alvensleben, U. 2000, *ASP Conf. Ser.* 221: Stars, Gas and Dust in Galaxies, 179
- Grebel, E. K. 2000, *ASP Conf. Ser.* 221, 297
- Grebel, E. K. 2001, *Dwarf galaxies and their environment*, 45
- Kong, X. 2000, *PASP*, 112, 1502
- Kong, X. & Cheng, F. Z. 2001, *MNRAS*, 323, 1035
- Kong, X. & Cheng, F. Z. 2002a, *A&A*, 389, 845
- Kong, X., Cheng, F.Z., Weiss, A., Charlot, S. 2002b, *A&A*, 396, 503
- Lejeune, T. & Schaerer, D. 2001, *A&A*, 366, 538
- Leitherer, C. et al. 1996, *PASP*, 108, 996
- Leitherer, C. et al. 1999, *ApJS*, 123, 3
- Marigo, P., Girardi, L., Groenewegen, M. A. T., & Weiss, A. 2001, *A&A*, 378, 958
- Mas-Hesse, J. M. & Kunth, D. 1999, *A&A*, 349, 765
- Metropolis N., Rosenbluth A., Teller A., Teller E., 1953, *J. of Chem. Phys.*, 21, 1087.
- Moeller, C. S., Fritze-v. Alvensleben, U., & Fricke, K. J. 1997, *A&A*, 317, 676
- Oconnell, R. W. 1976, *ApJ*, 206, 370
- Oestlin, G., Bergvall, N., & Roennback, J. 1998, *A&A*, 335, 85
- Olofsson, K. 1995, *A&AS*, 111, 57
- Olive, K. A. & Skillman, E. D. 2001, *New Astronomy*, 6, 119
- Papaderos, P., Izotov, Y. I., Thuan, T. X., Noeske, K. G., et al. 2002, *A&A*, 393, 461
- Pelat, D. 1998, *MNRAS*, 299, 877
- Pickles, A. J. 1985, *ApJ*, 296, 340
- Popescu, C. C. & Hopp, U. 2000, *A&AS*, 142, 247
- Rosa-González, D., Terlevich, E., & Terlevich, R. 2002, *MNRAS*, 332, 283
- Schaerer, D., Contini, T., & Pindao, M. 1999, *A&AS*, 136, 35
- Schmidt, A. A., Copetti, M. V. F., Alloin, D., & Jablonka, P. 1991, *MNRAS*, 249, 766

- Schmitt, H. R., Bica, E., & Pastoriza, M. G. 1996, MNRAS, 278, 965
- Smith, C. R. & Grandy, W.T.Jr. 1985, Maximum-entropy and bayesian methods in inverse problems, Dordrecht : D.Reidel
- Smoker, J. V., Axon, D. J., & Davies, R. D. 1999, A&A, 341, 725
- Skillman, E. D. & Kennicutt, R. C. 1993, ApJ, 411, 655
- Spinrad, H. & Taylor, B. J. 1971, ApJS, 22, 445
- Thuan, T. X. & Izotov, Y. I. 2000, IAU Symposium, 198, 176
- Vazdekis, A. & Arimoto, N. 1999, ApJ, 525, 144
- Weiss, A., Peletier, R. F., & Matteucci, F. 1995, A&A, 296, 73
- Westera, P., Lejeune, T., Buser, R., Cuisinier, F., & Bruzual, G. 2002, A&A, 381, 524
- Worthey, G. 1994, ApJS, 95, 107
- Worthey, G. & Ottaviani, D. L. 1997, ApJS, 111, 377

Table 4: Empirical population synthesis results of the galaxies with asymptotic (young-star) metallicities  $[Z/Z_{\odot}] = 0.0$ : percentage contribution to  $F_{\lambda 5870}$ .

$[Z/Z_{\odot}]$	$[Z/Z_{\odot}] = 0.0$					$-1.0$	$-1.5$	$-2.0$	$EW_{abs}(A)$				
Age(yr)	HII	E7	5E7	E8	5E8	E9	5E9	E10	$A_V$	H $\delta$	H $\gamma$	H $\beta$	H $\alpha$
Name	35	33	29	25	21	18	13	7					
vzw155	9.6	6.2	9.2	7.7	20.2	15.7	17.9	13.5	.24	4.45	2.68	3.78	1.61
iiiizw42	16.4	7.2	12.7	8.4	15.1	11.6	14.5	14.1	.54	4.35	2.57	3.80	1.44
zw0855	11.5	2.5	7.5	9.0	49.7	15.0	2.4	2.5	.03	3.59	3.06	3.50	-.07
iizw44	6.7	5.6	7.2	5.5	20.0	15.7	23.8	15.6	.21	4.49	3.50	4.72	1.43
mrk213	5.9	5.1	6.3	5.8	20.4	18.4	22.2	15.8	.46	4.42	3.46	4.67	1.55
iizw67	4.9	4.2	4.0	3.6	9.4	20.7	33.4	19.8	.39	4.51	2.67	5.31	1.70
mrk241	7.3	4.1	10.5	7.8	18.5	14.7	17.6	19.5	.32	4.58	2.79	4.08	1.26
izw53	17.7	9.3	7.4	4.6	26.7	12.1	13.3	8.9	.24	3.77	3.23	3.64	1.00
izw56	9.3	7.7	9.1	5.6	10.5	13.1	24.3	20.5	.82	4.67	2.74	3.82	1.87
iizw71	1.6	2.8	7.0	5.9	53.7	13.7	9.4	5.8	.13	4.11	2.23	3.48	.34
izw97	7.1	2.5	14.2	16.0	31.8	10.5	7.4	10.4	.06	4.75	3.38	4.53	1.20
izw101	11.7	4.9	8.5	5.7	17.9	15.1	19.0	17.1	.45	4.16	2.86	3.56	1.50
mrk303	9.1	6.5	4.1	2.8	14.4	17.6	30.5	14.8	.23	4.23	2.99	4.02	1.87
zw2220	22.4	11.4	15.8	10.9	4.7	8.3	13.8	12.7	.45	4.56	3.38	3.97	1.54
ivzw142	9.1	9.7	4.0	3.2	24.9	19.8	19.7	9.7	.46	4.08	3.35	3.41	1.32